Available online at www.sciencedirect.com
ScienceDirect
Combustion and Flame 150 (2007) 54–59
Combustion and Flame
www.elsevier.com/locate/combustflame

On mathematical modelling of flameless combustion

Marco Mancini [a], Patrick Schwöppe [a], Roman Weber [a,*], Stefano Orsino [b]

[a] *IEVB Institute, Clausthal University of Technology, Germany*
[b] *Fluent Inc., Lebanon, USA*

Received 29 May 2006; received in revised form 29 December 2006; accepted 20 March 2007

Available online 30 April 2007

Abstract

A further analysis of the IFRF semi-industrial-scale experiments on flameless (mild) combustion of natural gas is carried out. The experimental burner features a strong oxidizer jet and two weak natural gas jets. Numerous publications have shown the inability of various RANS-based mathematical models to predict the structure of the weak jet. We have proven that the failure is in error predictions of the entrainment and therefore is not related to any chemistry submodels, as has been postulated.
© 2007 The Combustion Institute. Published by Elsevier Inc. All rights reserved.

Keywords: Mild/flameless combustion; NO_x emissions

1. Introduction

Our paper is concerned with rapidly developing combustion technology [1] that has been given different names; high-temperature air combustion (HTAC [2]), mild combustion [3–5], or flameless oxidation [6]. The essence of this technology is that fuel is oxidized in an environment that contains a substantial amount of inert (flue) gases and some, typically not more than 3–5%, oxygen. For clean gaseous fuels that do not contain any fuel-bound nitrogen, this results in very low NO_x emissions even if the combustion air stream is preheated to temperatures in excess of 1000 °C.

There are several methods of realization of this combustion technology, as underlined in Refs. [1,4], and two, perhaps the most common ones, are described below. In the first method (see Refs. [1,2]), the combustion air is provided by a central, strong (high-momentum) air jet that is surrounded by a number of weak (low-momentum) fuel jets (in industrial applications typically two jets are used). These weak fuel jets are positioned away from the central air jet in order to inject the fuel into recirculated combustion products and, by doing so, to dilute the fuel before it mixes with the combustion air stream. The second method is recognized in the literature as a "classical" method of achieving flameless combustion [6]. It can be characterized by a central fuel jet and a number of air jets positioned in the relative vicinity of the central fuel jet.

Predicting performance of industrial devices that utilize the mild combustion principle is complex, since in addition to considerations on combustion chemistry, the fluid flow and mixing between fuel, oxidizer, and combustion products have to be considered. The publications leading to both the development and validation of such models can be split into these concerned with the strong jet–weak jet design and those concerned with a multiplicity of jets of similar momentum. In conjunction with the work of the

* Corresponding author. Fax: +49 5323 72 48 63.
E-mail address: roman.weber@ievb.tu-clausthal.de (R. Weber).

0010-2180/$ – see front matter © 2007 The Combustion Institute. Published by Elsevier Inc. All rights reserved.
doi:10.1016/j.combustflame.2007.03.007

first group, a unique set of measured data was generated [1,7]. The availability of these data initiated a number of publications aiming at both the development and validation of several mathematical models. In all these publications, the Reynolds–averaged Navier–Stokes (RANS) approach was retained; however, the works differed in the turbulence models or in turbulent-combustion interaction submodels used or in both. In Mancini et al. [8], the standard k–ε turbulence model was used together with three combustion submodels: the eddy-breakup model with a two-step reaction scheme, the eddy-dissipation concept model with chemical equilibrium, and the pdf/mixture fraction model with nonadiabatic lookup tables (for details of the NO postprocessor see Ref. [8]). With the exception of the fuel jet, the computations resulted in predictions of good quality. The predicted NO_x furnace emissions were in very good agreement with the measured values for a number of combustion-model/NO_x postprocessor combinations. However, the models failed to predict the structure of the weak jet. More precisely, within the fuel jet, the computed temperatures were typically 500–600 °C lower than the measured values and the predicted CH_4, CO_2, and CO concentrations differed by a factor of 2–3 from the measured values. Dong [9] used a RANS model based on k–ε equipped with a mixture fraction/pdf submodel to simulate the same experiments [1,7] and his predictions suffered exactly the same deficiency. More recently, Awosope et al. [10,11] used a Borghi diagram [12] to identify the combustion regimes of the considered experiments [1,7]. They used a combustion submodel that included the transport equations for the mean mixture fraction, its variance, and the mean reaction progress variable. The source term in the reaction progress variable was modeled following the work of Lindstedt and Vaos [13], which includes the influence of strain on the flamelets by small eddies. The flamelet functions were obtained from a priori computed lookup tables. Similarly to the models of Mancini et al. [8] and Dong [9], the model of Awosope et al. [10,11] also failed to predict the structure of the weak fuel jet. Notwithstanding the fact that perhaps a more thorough analysis of the applicability of the above-listed chemistry–turbulence models of the IFRF experiments [1,7] is required, as initiated by Awosope [10,11], one cannot refrain from observing that the more sophisticated the chemistry–turbulence model is, the worse are the predictions of the low-momentum fuel jet.

2. Objectives

The goal of this paper is to resolve the issue of the poor-quality predictions for the weak fuel jet. The main question is whether (new) low-temperature chemical kinetics schemas are really needed to improve the predictions in this flame region. Such a significant discrepancy between the predictions and the measurements in the fuel jet should have resulted in error predictions of the furnace exit NO emissions. To the contrary, all the NO postprocessors have predicted the furnace NO exit values with relatively good accuracy. To explain this rather surprising mathematical model effect, we use the IFRF measurements [1,7], several RANS models, and the radical chemistry mechanism (GRI Mech 3.0 [14]) incorporated into the Chemkin code.

3. The measured data

The in-furnace measured data used in this paper originate from the IFRF experiments [1,7] carried out in a refractory lined furnace with a 2×2 m cross section and a length of 6.25 m (see Fig. 1 in Ref. [7]). The furnace was equipped with one (0.58-MW thermal input) burner operated under steady state conditions. The burner consisted of a central oxidizer jet (named also comburent jet) and two natural gas injectors positioned 28 cm away from the central jet. A gaseous stream, of temperature 1573 K, containing 19.5% wet O_2, 59.1% wet N_2, 15% wet H_2O, and 6.4% wet CO_2, was supplied into the furnace through the central jet. This oxidizer stream (830 kg/h) contained also 94 vppm of NO calculated on a wet basis (110 vppm, dry). The volumetric composition of the furnace exit gases was 1.6% O_2, 27.3% H_2O, 13.7% CO_2, 57.7% N_2 and 102 ppm of NO (140 vppm, dry). The "net" NO production rate in the furnace is 0.06 g/kg of fuel. Detailed mapping of the turbulent velocities, temperatures, and chemical composition (O_2, CO, CO_2, CH_4, H_2, NO, and NO_x) as well as radiation has been reported elsewhere [1,7].

4. Mathematical models

4.1. The RANS mathematical models

For predicting the measured data we use several RANS models. The turbulence is modeled using either a standard k–ε model or a RNG k–ε model (more elaborate Reynolds transport models were also tested and only minor changes were observed). We use three combustion submodels listed in Table 1. The eddy-breakup submodel with a two-step reaction scheme [15] is the most simple one (model **1** in Table 1). The second submodel (the standard Fluent 5 CFD code) is based on a mixture-fraction transport equation that is equipped with nonadiabatic lookup

Table 1
Measured and predicted values

	Measurements [1,16]	Predictions using model no./run no.				
		1	**2**	**3**	**4**	**5**
Furnace exit temperature (K)	1493	1519	1498	1489	1480	1489
Furnace exit O_2 (%, vdry)	2.2	1.8	2.14	2.2	2.1	2.19
Furnace exit NO (ppmvd)	140	137	130	129	140	135
Furnace exit CO (ppmvd)	0	0	8	10	15	13
Peak temperature (K)	1808	1948	1973	1922	1770	1840
Peak H_2 (%, vdry)	1.97	9	13.1	10.9	2.5	2.0
Peak CO (%, vdry)	3.23	21	33	28	3.1	2.8

Note. **1**—IFRF-EBU [15] model; **2**—Fluent 5-pdf (mixture fraction) [17]; **3**—Fluent 5-pdf (mixture fraction)—fluctuations of the mixture fraction have been switched off; **4**—reactor network model with GRI 3.0 mechanism and entrainment calculated using RANS model-1; **5**—reactor network model with GRI 3.0 mechanism and entrainment estimated from the measured data.

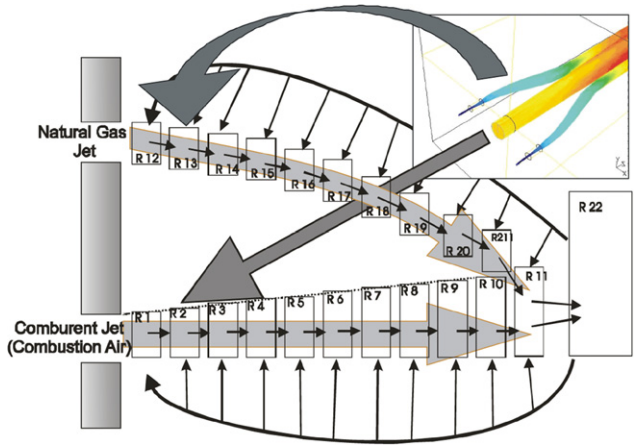

Fig. 1. Series of perfectly stirred reactors representing the strong jet (reactors R1–R10) and the weak jet (reactors R12–R21).

tables (model **2** in Table 1). In the third submodel, the turbulent fluctuations are switched off, but otherwise its formulation is identical to model **2**. To each of the above combustion submodels the same NO_x postprocessor is appended. The thermal and prompt NO are calculated in the same way as in Ref. [15], with no changes to any of the model parameters and constants. However, an extra NO-reburning path following the work of Chen [16] and De Soete [17] was added, as explained in Ref. [8]. Although we use the Chen NO reburning model, we realize that in the light of the present knowledge of NO precursors [18] the model does not have a firm scientific basis.

4.2. Series of perfectly stirred reactors

To provide the background for the detailed analysis of the chemistry, we have subdivided the flow into a network of perfectly stirred reactors (PSRN). We have divided the strong central jet into 10 reactors marked in Fig. 1 as R1–R10. Each reactor is of the same length and its width is determined by the position of the zero axial velocity, which is determined by the jet expansion angle. The location of this zero-axial-velocity line is known from both the measurements and the RANS predictions. The weak natural gas jet is divided into 10 PSRs marked in Fig. 1 as R12–R21. The streams leaving the fuel jet reactor R21 and the center jet reactor R10 merge into reactor R11. The rest of the furnace is represented by reactor R22. As has been shown in Fig. 1, reactors entrain hot recirculating combustion products that originate from the last reactor (R22). The inlet to the R12 reactor is a $47/2 = 23.5$ kg/h flow of natural gas of the following volumetric composition: 0.88 CH_4, 0.05 C_2H_6, 0.02 C_3H_8, 0.04 N_2. The inlet to R1 reactor is a $830/2 = 415$ kg/h comburent flow of the volumetric composition specified previously. We stress here again that this stream contains 94 vppm (wet) NO. The network of the reactors is solved using the CHEMKIN 3.7 computer code [19] with the GRI 3.0 reaction scheme for methane/air flames [14].

As shown in Fig. 1, both jets entrain combustion products of reactor R22 and we use two methods for determination of this entrainment. Since a RANS model solution is obtained, a simple integra-

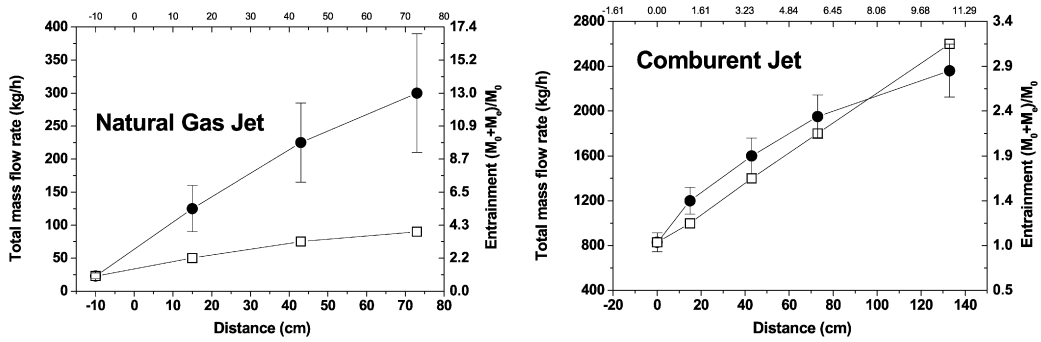

Fig. 2. Entrainment of the jets; left—the weak natural gas jet, right—the strong comburent jet; (●) entrainment estimated using the measured data [1,16]—the error bars indicate the inaccuracies in estimating the entrainment; (□) entrainment calculated using RANS model-1.

tion provides the entrainment values. Fig. 2 shows the entrainment, for both the weak and the strong jets, obtained using the RNG k–ε based RANS model-1 of Table 1. In the second method we use measured data that include the time-mean and fluctuating velocities (laser Doppler anemometry) and the time-mean temperatures and gas composition. These data have been collected point by point at several traverses in the symmetry plane cutting trough the middle of the furnace. Using these data, we have calculated the entrainment rates for both jets. Since the strong central jet remains axisymmetric and "stiff," with well-defined boundaries, this procedure is accurate and, as is shown in Fig. 2, the entrainment rates calculated from the measured data agree well with the RANS predictions. The same procedure has been applied to the weak jet of natural gas. Since the weak jet is strongly tilted toward the center jet, our procedure for calculating the entrainment using the measured data is in this case less accurate. The accuracy with which we estimate the entrainment rates is shown in Fig. 2 using the error bars. The same figure shows that there is a substantial discrepancy between the RANS model-1 predicted (other RANS models provide similar entrainment rates) and the "measured" entrainment.

5. Results and discussion

Table 1 shows the comparison between the measurements and predictions in terms of the furnace exit values. Excellent agreement is obtained for all the models used. The overall mass and energy balance (including radiation balance) is satisfied with an accuracy better than 0.5% for all the computational runs. It is worth noting that simple chemical equilibrium calculations, carried out for the furnace inlet conditions and for the furnace exit temperature of 1493 K and 1 bar pressure, result in NO emissions of 392 ppmvd, while 140 ppmvd was measured.

Fig. 3 shows the predicted temperature and oxygen in both jets using the RANS model-1 and the reactor network model, while Fig. 4 shows the NO and NO_2 concentrations within both jets. The predictions using RANS models **2** and **3** (see Table 1), show similar results in the fuel jet and are not plotted. For the reactor network model the entrainment figures are essential model inputs and therefore two computational runs are performed. In run 4 (Table 1) the entrainment is obtained using the RANS model-1 predictions, while in run 5 (Table 1) the entrainment is estimated directly from the measured data (see Fig. 2). Thus, in run 5 (Table 1), the entrainment into the fuel jet, at the point of merging into the comburent jet, is larger than in run 4 by a factor of 3.

The central jet is easy to predict, as shown in Figs. 3 and 4. Until a distance of around 70 cm, which corresponds to the R11 reactor, there are no combustion reactions taking place in the jet and its temperature is determined by the energy balance, which includes the entrainment and the radiation losses. The oxygen content in the jet decreases linearly with the distance due to the entrainment. Similarly, the NO concentration increases slightly with the distance, and this effect is again exclusively due to the entrainment.

Consider now the weak jet. Fig. 3 shows the predictions in the fuel jet obtained using the reactor network models (runs 4 and 5, Table 1). The flow rate of CH_4 leaving the fuel injector is 5.055 g/s. The CH_4 flow rate at the exit of reactor 21 is calculated to be 5.0335 g/s in run 4 while, for run 5, a figure of 4.84 g/s is applicable. The oxygen concentration in reactor 21 is calculated to be 1.21 and 1.3 vol% for runs 4 and 5, respectively. In run 4, only 0.43% of CH_4 is converted, in the fuel jet, into the intermediate radicals and CO (0.2% CO), while, for run 5, the corresponding figures are 4.3% of CH_4 and 0.933% CO, respectively. Thus, there is hardly any "consumption of fuel" taking place within the fuel jet. The

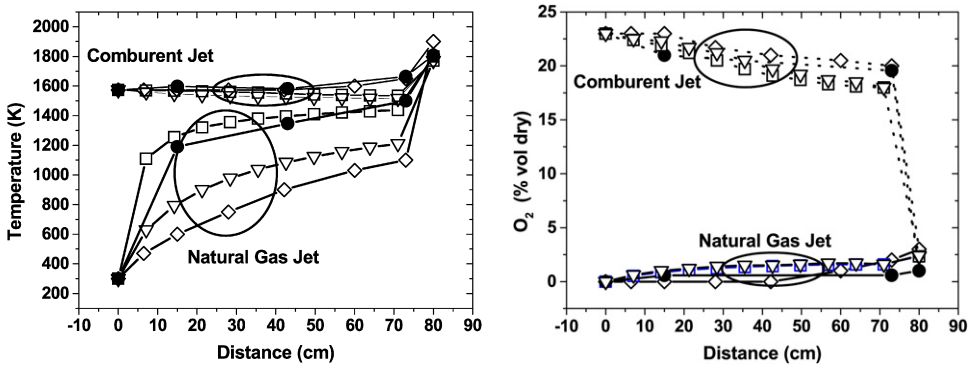

Fig. 3. Temperature (left) and O_2 (right) in the jets: (●) measurements [1,16]; (◇) RANS model-1 predictions; (▽) reactor network model with RANS model-1 computed entrainment; (□) reactor network model with entrainment estimated from the measured data (see Fig. 2).

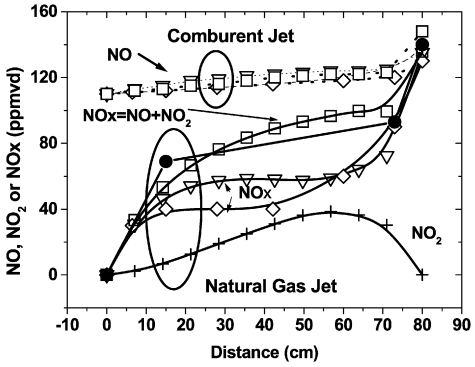

Fig. 4. NO concentrations in the jets: (●) NO_x measurements [1,16]; (◇) RANS model-1 predictions; (▽) reactor network model with RANS mode-1 computed entrainment; (□) reactor network model with entrainment estimated from the measured data (see Fig. 2); (+) NO_2–reactor network model with entrainment estimated from the measured data (see Fig. 2).

above analysis and run 5 temperature plot, shown in Fig. 3 (left), clearly demonstrate that the temperature increase within the fuel jet results almost exclusively from the entrainment of the hot combustion products. The process taking place within the fuel jet can be perhaps named "preconditioning" of the fuel. This process results in a fuel that is highly diluted with CO_2 and H_2O and is preheated to a temperature that is typically only 200–300 K lower than the temperature of around 1800 K under which the main fuel oxidation reactions proceed in reactor 11. In run 5, we have calculated that such a preconditioned fuel is of the following composition: $CH_4 = 5.3\%$, $H_2 = 0.5\%$, $CO_2 = 13.5\%$, $H_2O = 27.8\%$, and $N_2 = 50.9\%$. The reactor network model shows no NO formation within the fuel jet and its presence there is exclusively due to the entrainment. The NO_2, which is present in significant quantities within the fuel jet, is formed from the entrained NO via reactions $NO + O + M = NO_2 + M$ and $NO + HO_2 = NO_2 + OH$ (the first reaction provides around two-thirds of the NO_2 produced).

6. Conclusions

We have performed a further analysis of the semi-industrial-scale experiments [1,7] on mild (flameless) combustion of natural gas. The experimental burner has featured a strong (high-momentum) oxidizer jet and two weak (low-momentum) natural gas jets. It has been observed that little combustion occurs in the fuel jet. The temperature rise and the increasing NO concentrations along the fuel jet are almost exclusively due to the entrainment of hot combustion products. It has been proven that the failure of a number of RANS models in predicting the structure of the fuel jet is a result of error in predictions of the entrainment and therefore is not related to any chemistry submodels. The novelty of this paper is in showing that little combustion occurs within the natural gas jet. The temperature increase within the fuel jet results almost exclusively from the entrainment of the hot combustion products.

The process taking place within the fuel jet can be named "preconditioning" of the fuel and it results in a mixture containing around 6% of combustibles, 2% of oxygen, and 92% of inert gases (CO_2, H_2O, N_2). The mixture does not ignite until it merges into the oxidizer jet. Consequently, there is no NO formation within the fuel jet and its presence there is exclusively due to the entrainment.

References

[1] R. Weber, A.L. Verlaan, S. Orsino, N. Lallemant, J. Inst. Energy 72 (1999) 77–83.

[2] H. Tsuji, A. Gupta, T. Hasegawa, M. Katsuki, K. Kishimoto, M. Morita, High Temperature Air Combustion, CRS Press, New York, 2003.

[3] M. De Joannon, A. Cavaliere, T. Faravelli, E. Ranzi, P. Sabia, A. Tregrossi, Proc. Combust. Inst. 30 (2005) 2605–2612.

[4] A. Cavaliere, M. De Joannon, Prog. Energy Combust. Sci. 30 (2004) 329–366.

[5] R. Weber, J.P. Smart, W. van der Kamp, Proc. Combust. Inst. 30 (2005) 2623–2629.

[6] J.A. Wünning, J.G. Wünning, Prog. Energy Combust. Sci. 23 12 (1997) 81–94.

[7] R. Weber, S. Orsino, N. Lallemant, A. Verlann, Proc. Combust. Inst. 28 (2000) 1315–1321.

[8] M. Mancini, R. Weber, U. Bollettini, Proc. Combust. Inst. 29 (2002) 1155–1163.

[9] W. Dong, Design of advanced industrial furnaces using numerical modelling method, Ph.D. thesis, The Royal Institute of Technology, Stockholm, Sweden, 1999.

[10] I.O. Awosope, Flameless oxidation combustion modelling and application to a gas turbine combustor, Ph.D. thesis, Mechanical Engineering Department, Imperial College London, UK, 2005.

[11] I.O. Awosope, N.H. Kandamby, F.C. Lockwood, J. Energy Inst. 79 (2) (2006) 75–83(9).

[12] R. Borghi, Prog. Energy Combust. Sci. 14 (1988) 245–292.

[13] P. Lindstedt, E. Vaos, Combust. Flame 116 (1999) 461–485.

[14] Gas Research Institute, GRI-Mech, Ver. 3.0, http://www.me.berkely.edu/gri_mech/.

[15] A. Peters, R. Weber, Combust. Sci. Technol. 110–111 (1995) 67–101.

[16] W. Chen, A Global Reaction Rate for Nitric Oxide Reburning, Ph.D. thesis, Bringham Young University, 1994.

[17] G.G. De Soete, Proc. Combust. Inst. 15 (1975) 1093–1102.

[18] S. Song, K. Hanson, C.T. Bowman, D.M. Golden, Proc. Combust. Inst. 28 (2000) 2403–2409.

[19] R.J. Kee, F.M. Rupley, J.A. Miller, The CHEMKIN Thermodynamic Data Base; Sandia Report, SAND87-8215.